

Statistical properties of an enstrophy conserving finite element discretisation for the stochastic quasi-geostrophic equation

Thomas M. Bendall and Colin J. Cotter

March 14, 2022

Abstract

A framework of variational principles for stochastic fluid dynamics was presented by Holm (2015), and these stochastic equations were also derived by Cotter et al. (2017). We present a conforming finite element discretisation for the stochastic quasi-geostrophic equation that was derived from this framework. The discretisation preserves the first two moments of potential vorticity, i.e. the mean potential vorticity and the enstrophy. Following the work of Dubinkina and Frank (2007), who investigated the statistical mechanics of discretisations of the deterministic quasi-geostrophic equation, we investigate the statistical mechanics of our discretisation of the stochastic quasi-geostrophic equation. We compare the statistical properties of our discretisation with the Gibbs distribution under assumption of these conserved quantities, finding that there is agreement between the statistics under a wide range of set-ups.

1 Introduction

In recent years, there has been increased interest in stochastic models of geophysical fluids, as they provide a way to allow models to express some of the spread in uncertainty of unresolved processes. One approach is the variational principles framework introduced by [1] for stochastic fluid dynamics. In this framework, stochastic perturbations (representing the effect of unresolved motions on the resolved scales) are introduced as perturbations to the velocity field that transports Lagrangian fluid particles. This is expressed as in the following formula describing stochastic Lagrangian transport,

$$d\mathbf{x}_t = \mathbf{u}(\mathbf{x}, t) dt - \sum_i \boldsymbol{\Xi}_i(\mathbf{x}) \circ dW_i, \quad (1.1)$$

where \mathbf{u} is the deterministic velocity field, $\boldsymbol{\Xi}_i(\mathbf{x})$ are time-independent basis functions which determine the spatial correlations in the stochastic component of the velocity field, and $\circ dW_i$ denotes Stratonovich noise. The stochastic variational principle leads to Eulerian fluid models, with stochastic multiplicative noise in the form of additional transport terms, that have a conserved potential vorticity; the addition of noise breaks the time-translation symmetry and hence they do not conserve energy. Unlike other approaches, the introduction of stochasticity through this framework still has a Kelvin circulation theorem since it preserves the particle relabelling symmetry. This framework can be used to develop potential vorticity conserving stochastic versions of all of the geophysical fluid dynamics models that have Hamiltonian structure: shallow

water equations, Boussinesq equations, anelastic, pseudo-compressible, compressible Euler, and so on. The dynamics resulting from this approach has also been derived by [?], who decomposed the deterministic Lagrangian flow map into slow, large-scale motions and fast, small-scale fluctuations, before using homogenization theory.

Two important potential applications of this approach are modelling unresolved subgrid backscatter onto resolved scales and in ensemble prediction and ensemble data assimilation, where the stochastic forcing can be used to reach other nearby trajectories that are physically realistic.

In this work our goal is to study the behaviour of the stochastic equation derived in [1]. We will consider one of the simplest members of this stochastic model hierarchy, the stochastic quasi-geostrophic (QG) equation,

$$dq + d\mathbf{x}_t \cdot \nabla q = 0, \quad q := \nabla^2 \psi - \mathcal{F}\psi + f, \quad (1.2)$$

where $q(\mathbf{x}, t)$ is the scalar potential vorticity, \mathcal{F} is the non-dimensional Froude number and f is the non-dimensional Coriolis parameter. The stream function ψ is related to the velocity \mathbf{u} through

$$\mathbf{u} = \nabla^\perp \psi,$$

where the ∇^\perp operator is defined by $\nabla^\perp := (-\partial_y, \partial_x)$.

Our approach is to study the new stochastic QG equation via numerical models, thereby proposing a first discretisation to this equation. In this paper we develop a conforming finite element discretisation for the stochastic QG equation, showing that it conserves total PV and enstrophy. Having presented a new discretisation, we then study its statistical mechanics in numerical experiments that compare the long time statistics of the model with predictions from an appropriate Gibbs distribution, which helps us to learn about the properties of the underlying stochastic QG equation. The novel results of this work are the presentation of a discretisation to the stochastic QG equation, using a standard finite element method with implicit midpoint rule time stepping, and the subsequent investigation of its statistical properties. Through this approach, we find that the equilibrium distribution in phase space of the numerical model is approximated by a Gibbs distribution. We also provide a derivation of the stochastic QG model directly from the stochastic variational principle using the Lagrangian of [2], contrasting with the Hamiltonian approach used in [1].

The rest of this paper is structured as follows. In Section 2 we derive the stochastic QG equation. In Section 3 we describe the finite element discretisation and derive conservation properties. In Section 4 we review the properties of the Gibbs distribution under the assumption of conservation of enstrophy, and in Section 5 we compare statistics from the numerical discretisation with corresponding statistics from the Gibbs distribution. Finally we provide a summary and outlook in Section 6.

2 Stochastic quasi-geostrophic model derivation

In this section we derive the stochastic QG equation from a stochastic variational principle, by adapting the variational principle for QG of [2] to the stochastic framework of [1]. This equation was previously only derived by [1] using a Poisson bracket approach. [2] considered a fluid with velocity \mathbf{u} and density ρ , together with a Lagrange multiplier P (which we will later use to

enforce constant density $\rho = \rho_0$ and hence incompressibility). Following the framework of [2], we construct the following action

$$\begin{aligned} S[u, \rho, \phi, \mathbf{p}, \mathbf{q}, P] = & \int \ell(\mathbf{u}, \rho, P) dt + \int_{\Omega} \phi \left(d\rho + \left[\mathbf{u} dt + \sum_i \boldsymbol{\Xi}_i(\mathbf{x}) \circ dW_i \right] \cdot \nabla \rho \right) \\ & + \mathbf{p} \cdot \left(d\mathbf{q} + \left[\mathbf{u} dt + \sum_i \boldsymbol{\Xi}_i(\mathbf{x}) \circ dW_i \right] \cdot \nabla \mathbf{q} \right) d^2x dt, \end{aligned} \quad (2.1)$$

where ℓ will be the Lagrangian, ϕ is a Lagrange multiplier enforcing the continuity equation, $\mathbf{q}(\mathbf{x}, t)$ is the back-to-labels map returning the Lagrangian label of the fluid particle at position \mathbf{x} at time t , and $\mathbf{p}(\mathbf{x}, t)$ is the Lagrange multiplier enforcing the advection of Lagrangian particles. The basis functions $\boldsymbol{\Xi}_i$ are tangential to the boundary $\partial\Omega$ of the domain Ω , which we shall assume to be simply connected.

Following [2], we use the specific Lagrangian for QG

$$\ell(\mathbf{u}, \rho, P) = \int_{\Omega} \left(\frac{1}{2} \rho |\mathbf{u}|^2 - \frac{1}{2} \mathcal{F} \rho \mathbf{u} \cdot \Delta^{-1} \mathbf{u} + \rho \mathbf{u} \cdot \mathbf{R} + P(\rho - \rho_0) \right) d^2x, \quad (2.2)$$

where \mathbf{R} is the fluid velocity due to the rotation of the planet so that $\hat{\mathbf{z}} \cdot \nabla \times \mathbf{R} = f$, and where the operator Δ^{-1} is the inverse of the Laplacian operator.

After computing the Euler-Lagrange equations and eliminating \mathbf{p} , \mathbf{q} and ϕ , computations in [1] lead to the equation

$$d \left(\frac{1}{\rho_0} \frac{\delta \ell}{\delta \mathbf{u}} \right) + d\mathbf{x}_t \cdot \nabla \left(\frac{1}{\rho_0} \frac{\delta \ell}{\delta \mathbf{u}} \right) + \frac{1}{\rho_0} \sum_k \frac{\delta \ell}{\delta u^k} \nabla dx_t^k + \nabla \frac{\delta \ell}{\delta \rho} dt = \mathbf{0}, \quad \frac{\delta \ell}{\delta P} = 0, \quad (2.3)$$

where $d\mathbf{x}_t$ is given in Equation (1.1) For the QG case this gives

$$\frac{1}{\rho_0} \frac{\delta \ell}{\delta \mathbf{u}} = \mathbf{u} + \mathbf{R} - \mathcal{F} \Delta^{-1} \mathbf{u}, \quad \frac{\delta \ell}{\delta \rho} = \frac{1}{2} |\mathbf{u}|^2 - \frac{1}{2} \mathcal{F} \mathbf{u} \cdot \Delta^{-1} \mathbf{u} + \mathbf{u} \cdot \mathbf{R} + P, \quad \rho = \rho_0. \quad (2.4)$$

Taking the curl of (2.3) and manipulating using vector calculus identities yields

$$(d + d\mathbf{x}_t \cdot \nabla) \left[\hat{\mathbf{z}} \cdot \nabla \times \left(\frac{1}{\rho_0} \frac{\delta \ell}{\delta \mathbf{u}} \right) \right] = 0.$$

For the QG reduced Lagrangian we compute

$$\begin{aligned} \hat{\mathbf{z}} \cdot \nabla \times \left(\frac{1}{\rho_0} \frac{\delta \ell}{\delta \mathbf{u}} \right) &= \hat{\mathbf{z}} \cdot (\nabla \times \mathbf{u}) + \hat{\mathbf{z}} \cdot (\nabla \times \mathbf{R}) - \mathcal{F} \Delta^{-1} \hat{\mathbf{z}} \cdot (\nabla \times \mathbf{u}), \\ &= \nabla^2 \psi - \mathcal{F} \psi + f, \end{aligned}$$

after substituting (2.4) and introducing the stream function ψ so that $\nabla^\perp \psi = \mathbf{u}$. The boundary conditions require that $\psi = 0$ on $\partial\Omega$. The resulting equation is

$$(d + d\mathbf{x}_t \cdot \nabla) [\nabla^2 \psi - \mathcal{F} \psi + f] = 0, \quad (2.5)$$

which is the stochastic QG equation for potential vorticity $q = \nabla^2 \psi - \mathcal{F} \psi + f$. This equation has an infinite set of conserved quantities,

$$C^p = \int_{\Omega} q^p d^2x,$$

for $p = 1, 2, 3, \dots$, with $p = 1$ corresponding to the total PV, and $p = 2$ is proportional to the enstrophy, which is given by $Z = \frac{1}{2} \int_{\Omega} q^2 \, d^2x$. Although the energy is not conserved, we can deduce that it remains bounded, since

$$\begin{aligned} 2E &= \int_{\Omega} (|\nabla\psi|^2 + \mathcal{F}\psi^2) \, d^2x, \\ &= \int_{\Omega} (f - q)\psi \, d^2x, \\ &\leq \left(\int_{\Omega} (f - q)^2 \, d^2x \right)^{1/2} \left(\int_{\Omega} \psi^2 \, d^2x \right)^{1/2}, \\ &\leq C \left(\int_{\Omega} q^2 \, d^2x \right)^{1/2} \left(2 \int_{\Omega} |\nabla\psi|^2 + \mathcal{F}\psi^2 \, d^2x \right)^{1/2}, \end{aligned}$$

with C a positive constant having used the Poincaré inequality, and hence

$$E \leq \sqrt{C/2} \int_{\Omega} q^2 \, d^2x, \quad (2.6)$$

and so E is bounded by a constant multiplied by the enstrophy, a positive constant of motion.

3 Finite element discretisation

In this section we present, for the stochastic QG equation, a discretisation that preserves the total PV and enstrophy. We use a finite element discretisation, which allows for the equation to be easily solved on arbitrary meshes, and in particular on the sphere.

The weak form of the stochastic QG equation is obtained by multiplying Equation (1.2) by a test function γ , and integrating by parts to obtain

$$d \int_{\Omega} \gamma q \, d^2x - \int_{\Omega} q \nabla \gamma \cdot \left(\nabla^{\perp} \psi \, dt + \sum_i \Xi_i(\mathbf{x}) \circ dW_i \right) \, d^2x = 0, \quad (3.1)$$

where the boundary term vanishes since $\mathbf{dx}_t \cdot \mathbf{n} = 0$ on $\partial\Omega$. A similar procedure, multiplying the relationship between ψ and q by a test function ϕ that vanishes on the boundary leads to

$$\int_{\Omega} (\mathcal{F}\phi\psi + \nabla\phi \cdot \nabla\psi) \, d^2x = \int_{\Omega} \phi(f - q) \, d^2x. \quad (3.2)$$

This is just the standard weak form for the Helmholtz equation.

We introduce a finite element discretisation by choosing a continuous finite element space V , defining

$$\mathring{V} = \{\psi \in V : \psi = 0 \text{ on } \partial\Omega\}.$$

The finite element discretisation is obtained by choosing $(q, \psi) \in (V, \mathring{V})$ such that Equations (3.1)-(3.2) hold for all test functions $(\gamma, \phi) \in (V, \mathring{V})$.

It follows immediately from the weak form (3.1) that the total PV is conserved, since choosing $\gamma = 1$ leads to

$$d \int_{\Omega} q \, d^2x = 0.$$

The enstrophy is conserved since choosing $\gamma = q$ leads to

$$d \int_{\Omega} q^2 d^2x = 0.$$

Proof that the p -th moment is conserved requires taking $\gamma = q^{p-1}$, but this is not in V for $p > 2$ and thus higher moments are not conserved. In the absence of noise, this discretisation also conserves energy; it reduces to the standard vorticity-stream function finite element formulation. For time integration we use the implicit midpoint rule, and we obtain

$$\begin{aligned} & \int_{\Omega} \gamma (q^{n+1} - q^n) d^2x \\ & - \int_{\Omega} \frac{q^{n+1} + q^n}{2} \nabla \gamma \cdot \left(\nabla^{\perp} \psi^{n+1/2} \Delta t + \sum_i \Xi_i(\mathbf{x}) \Delta W_i \right) d^2x = 0, \quad \forall \gamma \in V, \\ & \int_{\Omega} \left(\mathcal{F} \phi \psi^{n+1/2} + \nabla \phi \cdot \nabla \psi^{n+1/2} \right) d^2x - \int_{\Omega} \phi \left(f - \frac{q^{n+1} + q^n}{2} \right) d^2x = 0, \quad \forall \phi \in \dot{V}, \end{aligned}$$

where ΔW_i are independent random variables with normal distribution, $N(0, \Delta t)$. This provides a coupled nonlinear system of equations for $(q^{n+1}, \psi^{n+1/2})$ which may be solved using Newton's method.

Taking $\gamma = 1$ immediately gives conservation of the total vorticity Π ,

$$\int_{\Omega} (q^{n+1} - q^n) d^2x = 0.$$

Since the implicit midpoint rule conserves all quadratic invariants of the continuous time equations, this scheme conserves the enstrophy Z exactly as well. The use of the implicit midpoint rule also makes the scheme unconditionally stable. The argument behind the bound of the energy of the previous section also holds when restricted to the finite element space, with a constant that is independent of mesh size.

4 Statistical Properties of the Numerical Scheme

One of our main goals in this work is to understand the properties of the discretisation presented in Section 3. We are particularly motivated by the work of [12] and [13], who looked at the statistical mechanics of discretisations of the deterministic equation but with randomised initial states. In particular, [13] looked at how the conservation properties of the discretisation could affect the statistics. In both cases, the distribution of states in phase space was given by a Gibbs distribution. It is therefore of interest whether this same approach could be applied to our discretisation of the stochastic QG equation, and whether this can still be described by the Gibbs distribution.

There is a long history of applying statistical mechanics to describe 2D flows, for instance see [3], [4], [5] or [6]. Some examples of the application to geophysical flows are [7] and [8], while there have also been statistical treatments of quasi-geostrophic fluids, such as [9], [10] and [11]. More recently, the statistical mechanics of numerical discretisations has been considered. [12] considered Fourier truncations of the QG equation, whilst [13] considered finite difference methods using Arakawa's Jacobian, conserving energy and enstrophy. [13] also considered the other

Arakawa schemes that conserve energy but not enstrophy, or conserve enstrophy but not energy, and compared the numerical results with statistics from Gibbs distributions derived under those assumptions. Since the stochastic QG equation in our finite element discretisation does not conserve energy but does conserve enstrophy, we are actually in exactly this second situation. Following that paper, from the maximum entropy principle with constraints of conserved total vorticity Π and enstrophy Z , we find that the invariant distribution for the finite element discretisation is the Gibbs distribution $\mathcal{G}(\mathbf{Q})$, where \mathbf{Q} is the vector of values describing the discrete q field. For our numerical scheme the probability density function for this Gibbs distribution is

$$\mathcal{G}(\mathbf{Q}) = C^{-1} \exp[-\alpha (Z(\mathbf{Q}) + \mu\Pi(\mathbf{Q}))], \quad (4.1)$$

where C , α and μ are parameters providing the constraints of conserved Π , conserved Z and that the integral of the distribution is unity.

In this paper, we are interested in computing statistics from this distribution and comparing them to what is obtained from time averages over numerical solutions from the finite element discretisation. For example, the expectation of the energy E of the system is then

$$\langle E \rangle = \int_{\mathbb{R}^N} E(\mathbf{Q}) \mathcal{G}(\mathbf{Q}) \, d\mathbf{Q}. \quad (4.2)$$

In general it is not possible to compute this integral analytically. Our approach is therefore to sample the distribution using a Metropolis algorithm.

Before we do this, we will decompose the state vector \mathbf{Q} into stationary and fluctuating parts:

$$\mathbf{Q} = \langle \mathbf{Q} \rangle + \mathbf{Q}'. \quad (4.3)$$

The components $\{Q_i\}$ of \mathbf{Q} are the coefficients in the finite element discretisation, so that for finite element basis $\{\phi_i\}$ with N components,

$$q = \sum_i^N Q_i \phi_i(\mathbf{x}).$$

Dubinkina and Frank showed in [13] that the average values $\langle Q_i \rangle$ took a constant value. Following their computation, we evaluate

$$\left\langle \frac{\partial Z}{\partial \mathbf{Q}} + \mu \frac{\partial \Pi}{\partial \mathbf{Q}} \right\rangle_{\mathcal{G}} = \int_{\mathbb{R}^N} \left(\frac{\partial Z}{\partial \mathbf{Q}} + \mu \frac{\partial \Pi}{\partial \mathbf{Q}} \right) C^{-1} \exp[-\alpha(Z(\mathbf{Q}) + \mu\Pi(\mathbf{Q}))] \, d\mathbf{Q}.$$

Inspection of the right hand side reveals that

$$\left\langle \frac{\partial Z}{\partial \mathbf{Q}} + \mu \frac{\partial \Pi}{\partial \mathbf{Q}} \right\rangle = -\alpha^{-1} \int_{\mathbb{R}^N} \frac{\partial}{\partial \mathbf{Q}} \mathcal{G}(\mathbf{Q}) \, d\mathbf{Q},$$

and if $\mathcal{G}(\mathbf{Q})$ decays sufficiently fast at infinity then we conclude that

$$\left\langle \frac{\partial Z}{\partial \mathbf{Q}} + \mu \frac{\partial \Pi}{\partial \mathbf{Q}} \right\rangle = \mathbf{0}. \quad (4.4)$$

In the finite element discretisation with domain Ω , $\Pi(\mathbf{Q})$ and $Z(\mathbf{Q})$ are given by

$$\Pi(\mathbf{Q}) = \sum_i^N \int_{\Omega} \phi_i(\mathbf{x}) Q_i \, d^2x, \quad Z(\mathbf{Q}) = \frac{1}{2} \sum_{i,j}^N Q_i Q_j \int_{\Omega} \phi_i(\mathbf{x}) \phi_j(\mathbf{x}) \, d^2x. \quad (4.5)$$

Substituting these into (4.4) gives

$$\left\langle \int_{\Omega} \phi_i(\mathbf{x})(Q(\mathbf{x}) + \mu) \, d^2x \right\rangle = 0, \quad \forall \phi_i.$$

This means that $Q(\mathbf{x})$ is the L^2 -projection of the constant function $\mu \times 1$ into V , but $\mu \times 1 \in V$, and we conclude that $\langle Q(\mathbf{x}) \rangle = -\mu$ for all i . For an initial value for the fluid simulation of $\Pi(\mathbf{Q}) = \mathcal{P}_0$, this gives $\langle Q_i \rangle = \mathcal{P}_0/A$, where $A = \int_{\Omega} d^2x$.

The significance of this result is that it is possible to use the Metropolis algorithm to generate samples from the distribution given in Equation (4.1) by taking samples from

$$\mathcal{G}'(\mathbf{Q}') = C^{-1} \exp[-Z(\mathbf{Q}')]. \quad (4.6)$$

This generates samples \mathbf{Q}' with $\langle \Pi(\mathbf{Q}') \rangle = 0$ and $\langle Z(\mathbf{Q}') \rangle = \mathcal{Z}'$, which can be transformed into samples of the desired distribution $\mathcal{G}(\mathbf{Q})$ (i.e. with $\langle \Pi(\mathbf{Q}) \rangle = \mathcal{P}_0$ and $\langle Z(\mathbf{Q}) \rangle = \mathcal{Z}_0$) by taking

$$Q_i = \frac{\mathcal{P}_0}{A} + Q'_i \sqrt{\frac{\mathcal{Z}_0}{\mathcal{Z}'} - \frac{\mathcal{P}_0^2}{2A\mathcal{Z}'}}. \quad (4.7)$$

The Metropolis algorithm can therefore be used to take samples from $\mathcal{G}'(\mathbf{Q})$, which avoids the evaluation of the parameter α in (4.1). The Metropolis algorithm finds to samples of $\mathcal{G}'(\mathbf{Q}')$ by generating samples from a similar, known distribution, $\mathcal{L}(\mathbf{Q}')$. A given sample \mathbf{Q}' is accepted to be from $\mathcal{G}'(\mathbf{Q}')$ if

$$\frac{\mathcal{G}'(\mathbf{Q}')}{c\mathcal{L}(\mathbf{Q}')} > 1, \quad (4.8)$$

where c is a prescribed constant greater than 1. The Metropolis algorithm also allows us to avoid evaluating the normalisation constants of the distributions. A more detailed description of the Metropolis algorithm can be found for example in [14].

The known distribution $\mathcal{L}(\mathbf{Q}')$ that we use is

$$\mathcal{L}(\mathbf{Q}') = C_{\mathcal{L}}^{-1} \exp[-Z_L(\mathbf{Q}')]. \quad (4.9)$$

The lumped enstrophy $Z_L(\mathbf{Q}')$ is defined as

$$Z_L(\mathbf{Q}') = \sum_{ij} \int_{\Omega} \frac{1}{2} Q_i^2 \phi_i(\mathbf{x}) \phi_j(\mathbf{x}) \, d^2x \equiv \sum_i \frac{1}{2} Q_i^2 M_i^L, \quad (4.10)$$

with lumped mass matrix $M_i^L := \sum_j \int_{\Omega} \phi_i(\mathbf{x}) \phi_j(\mathbf{x}) \, d^2x$. This distribution is now straightforward to sample, as

$$\mathcal{L}(\mathbf{Q}') = C_{\mathcal{L}}^{-1} \exp \left[- \sum_i^N \frac{1}{2} Q_i^2 M_i^L \right] = C_{\mathcal{L}}^{-1} \prod_i^N \exp \left[- \frac{1}{2} Q_i^2 M_i^L \right].$$

The known distribution is then sampled by generating coefficients Q'_i that are normally distributed with mean 0 and variance $1/M_i^L$.

Therefore samples of the Gibbs distribution $\mathcal{G}(\mathbf{Q})$ are found by using the Metropolis algorithm with the known $\mathcal{L}(\mathbf{Q}')$ to get samples of $\mathcal{G}'(\mathbf{Q}')$, and translating the samples \mathbf{Q}' using (4.7). It is important to note that in general a generated sample \mathbf{Q} will not have $\Pi(\mathbf{Q}) = \mathcal{P}_0$ and $Z(\mathbf{Q}) = \mathcal{Z}_0$. Instead the samples will have $\Pi(\mathbf{Q})$ and $Z(\mathbf{Q})$ distributed around \mathcal{P}_0 and \mathcal{Z}_0 . As the resolution increases, the distribution of samples will become tighter around the possible states in the discretisation.

5 Numerical Results

In this section we compute numerical trajectories of the finite element discretisation, and compare their time averages with statistics computed using the Gibbs-like distribution. The aim was to learn about the properties of the stochastic QG equation using this approach, and to show that the Gibbs-like distribution describes the distribution of the states of discretisation in phase-space, in the limit that the grid spacing goes to zero. The code was developed using the Firedrake software suite, which provides code generation from symbolic expressions [15].

5.1 Experimental Set-up

The tests were run on a sphere with unit radius, that is approximated using an icosahedral mesh. The resolution of this mesh can be refined by subdividing the triangular elements at a given resolution into four smaller triangles to obtain the next resolution. The refinement level of the icosahedron is the number of times this process has been repeated to form the mesh. The function space V was the space of continuous linear functions on these triangles, whose degrees of freedom (DOFs) are evaluation of the function at the cell vertices. The fluid simulation was run for T time steps of $\Delta t = 1$ and the Ξ functions were derived from stream functions given as the projections of the first nine spherical harmonics into the discrete streamfunction space. The strength of the stochastic part of the stream function (i.e. the multiplicative constant to the stochastic basis functions) was kept the same for each basis function. It was found not to affect the average values of the simulation, but increasing it did increase the speed with which the averaged values converged to their limits.

For the statistical simulation, the Gibbs-like distribution was used with Π and Z corresponding to the initial condition of the fluid simulation. At the first stage of the statistical simulation, n samples were generated to create an accurate approximation for \mathcal{Z}' to use in equation (4.7). Then the statistical simulation took n samples of the Gibbs-like distribution that were used for the comparison with the statistics of the fluid simulation. Average properties are found for each simulation by taking the mean value of each sample. In the case of the fluid simulation, the system at each time step is considered to be a sample.

5.2 Comparison of Mean Fields

As the simulations are run, this generates average states in which q is well-mixed over the domain. Figure 1 shows that the average values predicted from the fluid simulation and the Monte Carlo simulation lie very close to one another, even when the fluid simulation starts far from its average state. This figure plots the average Casimirs $\mathcal{C}_3 = \int_{\Omega} q^3 d^2x$ and $\mathcal{C}_4 = \int_{\Omega} q^4 d^2x$ as a function of the number of samples used in calculating that average for a single run of the simulation: we call this the *rolling average* of the simulations and denote it by angular brackets $\langle \cdot \rangle_t$. This plot was from a run at icosahedron refinement level 4 (corresponding to 2562 q DOFs), and the fluid simulation was initialised with $q = \sin \lambda$ for latitude λ .

We also took the rolling mean of different diagnostic fields. These were observed to converge to similar fields for both the statistical sampling and from solving the equations of motion. Figure 2 shows a comparison of the mean q^2 fields generated via each different method (this is more meaningful than the mean q field, which shows very little variation over the domain). The differences shown over the domain are due to the differences in area of the elements, whilst the fluid simulation results shown in (a) are slightly higher than those in (b) as at finite resolution

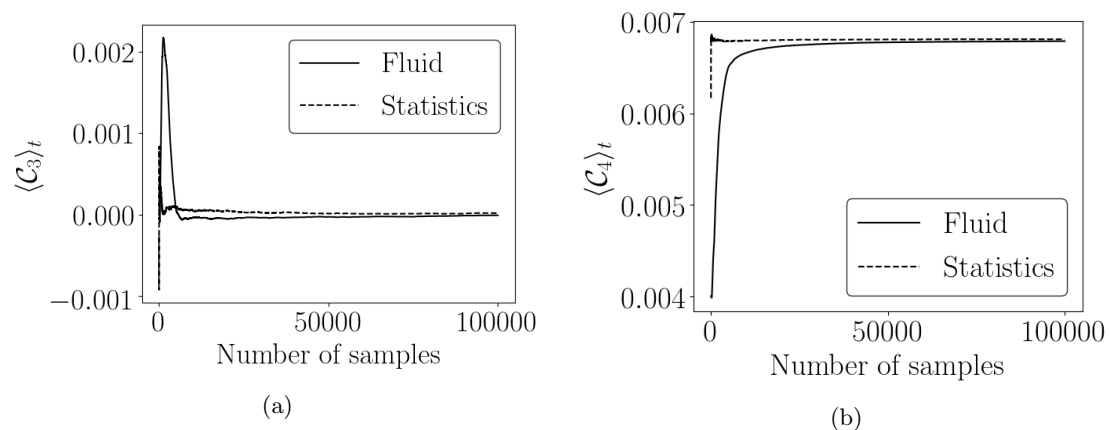


Figure 1: The evolution of the rolling average of the Casimirs (a) $C_3 = \int_{\Omega} q^3 d^2x$ and (b) $C_4 = \int_{\Omega} q^4 d^2x$ as the stochastic fluid simulation is run for 10^5 time steps and as 10^5 samples are taken from the Gibbs distribution. Both of these are plotted on the same axis, taking one time step of the fluid simulation to be one sample. The fluid simulation was run from an initial condition of $q = \sin \lambda$. We observe that both the rolling averages are both converging to the same values, as predicted by the statistical theory.

the value of Z of the Gibbs distribution is not exactly equal to that of the fluid simulation. As the resolution of the model is refined, the areas of the element will become closer together, and the deviations in the field over the domain should decrease. This was observed and is plotted in Figure 3.

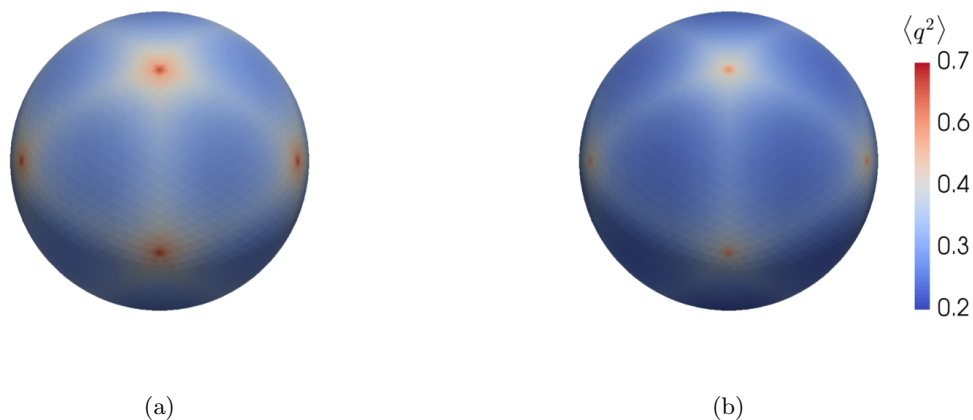
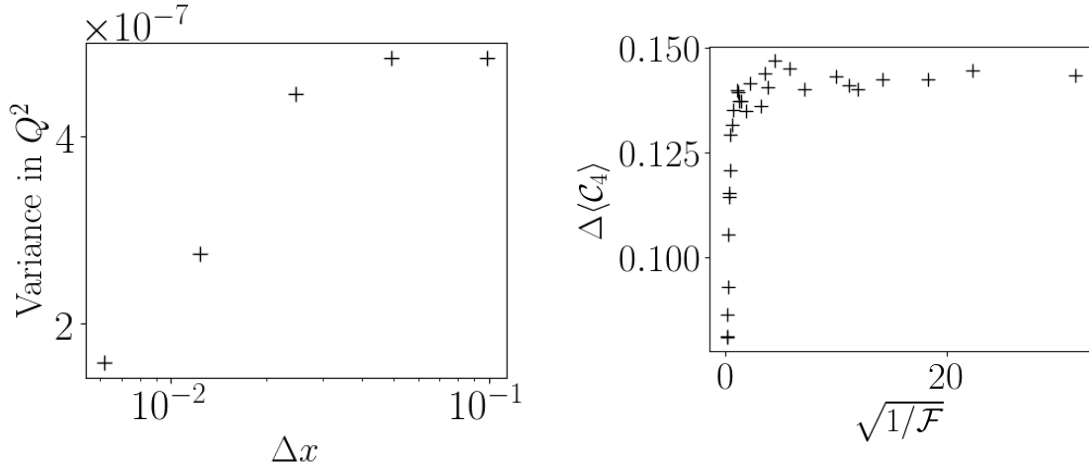


Figure 2: A comparison of the mean square potential vorticity q^2 field generated at icosahedron refinement level 4 (corresponding to 2562 q DOFs) by (a) the stochastic fluid simulation run for 10^5 steps with an initially random field and (b) 10^5 samples taken from the Metropolis algorithm. We observe that the two fields are essentially the same, as predicted by the statistical theory.



Figures 3 and 4: (Left) A plot of the final value of $\int_{\Omega} (q^2 - \bar{q}^2)^2 d^2x$ after 10^4 time steps at $\Delta t = 1$ of the fluid simulation, where $q^2 = \int_{\Omega} q^2 d^2x/A$ and $A = \int_{\Omega} d^2x$. This shows that as the resolution is increased, the variations in the mean q^2 field reduce. (Right) The rate of mixing (i.e., rate of convergence of statistics to the equilibrium values) of the fluid simulation as a function of the parameter \mathcal{F} , as measured by the speed at which the fourth Casimir \mathcal{C}_4 moves away from its initial value. Each point represents the difference at the 2000th time step of the ensemble mean value of \mathcal{C}_4 from its initial value. We observe that the rate of mixing is low for large \mathcal{F} , which corresponds to large (dimensionless) Rossby deformation radii. This is because scales that are below the Rossby deformation radius are effectively just transported by the flow field without feeding back, and so a large \mathcal{F} places more scales in this category.

5.3 The Effect of \mathcal{F}

The effect of the constant \mathcal{F} upon the convergence of the model was also investigated. The equations of motion were solved for a series of different values for \mathcal{F} . For each value of \mathcal{F} , the fluid model was run 50 times, creating an ensemble with different realisations of the noise. Our aim is to learn about the behaviour of the discretised stochastic QG equation by initialising the fluid at a state far from being well-mixed, and looking at the effect \mathcal{F} has on the rate of mixing under stochastic noise. The initial condition was chosen to be $q_0 = \sin \lambda$, which is a state far from a well-mixed equilibrium. This experiment was done with 2562 PV DOFs.

The difference between the initial value of \mathcal{C}_4 and its value for the ensemble average was recorded after $T = 2000$ time steps. We found that the average change in \mathcal{C}_4 over this time was a good proxy for the rate of mixing of the PV field: the larger the difference then the higher rate of mixing. This was plotted as a function of $1/\sqrt{\mathcal{F}}$, which describes a characteristic length scale. These values are displayed in Figure 4, which shows smaller differences for smaller length scales (or higher values of \mathcal{F}). This experiment was also performed at different resolutions, which showed the same behaviour.

5.4 Convergence With Resolution

While solving the equations of motion produces only samples with identical Π and Z , the samples taken from the Gibbs distribution will have different values of Π and Z , but spread about those values specified in the distribution. As the resolution is increased, samples taken from the Gibbs distribution should fit more tightly around the samples taken from solving the equations

of motion.

To investigate this we ran the fluid simulation and sampled the Gibbs distribution at various resolutions to produce histograms of various statistics. We took 10000 samples from the Gibbs distribution without scaling the resultant \mathbf{Q} field (i.e. the samples had $\langle \Pi(\mathbf{Q}) \rangle = 0$ and $\langle Z(\mathbf{Q}) \rangle = Z'$ as described in section 4, where Z' will be resolution dependent). This will correspond to a fluid simulation with an initial state of $\Pi = 0$ and $Z = Z'$. Histograms at different resolutions of the Π and Z values of the statistical samples are plotted in Figure 5. They have been normalised to remove the resolution dependence of Z' . The resultant histograms do indeed fit more tightly around the conserved fluid values as the resolution is increased. Figure 6 plots the standard deviation of these histograms as a function of resolution, which shows that the standard deviation converges linearly as a function of resolution. We also would expect to see similar behaviour for other statistics, although in the case of more complicated statistics such as variances or higher moments of the distribution, we expect that a very large number of samples will be required in order to observe this convergence.

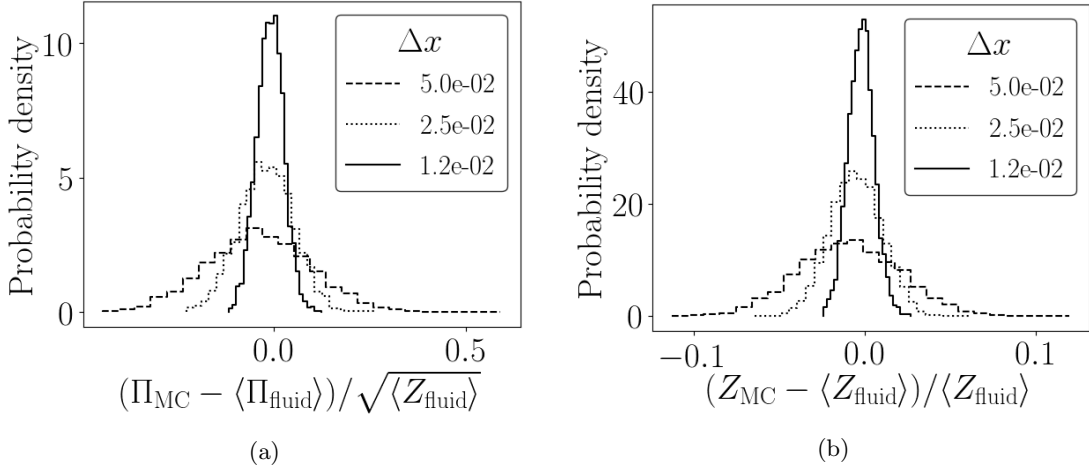


Figure 5: Histograms of the (a) $\Pi = \int_{\Omega} q \, d^2x$ and (b) $Z = \frac{1}{2} \int_{\Omega} q^2 \, d^2x$ values of different samples of the Gibbs distribution at three resolutions.

5.5 Topography

The fluid and statistical models also show the same properties when topography is included in the model. This is done by the addition of an extra term to the potential vorticity definition:

$$q := \nabla^2 \psi - \mathcal{F}\psi + f + h. \quad (5.1)$$

We performed similar experiments to those described above by mimicking an isolated mountain, as described as the fifth test case in [16]. In this case, the topography is described by the following function:

$$h = h_0(1 - r/R), \quad (5.2)$$

where $h_0 = 2$, $R = \pi/9$ and $r = \min [R^2, (\lambda - \lambda_c)^2 + (\theta - \theta_c)^2]$, for latitude λ and longitude θ . The centre of the mountain is at $\lambda_c = 3\pi/2$ and $\theta_c = \pi/6$. We also completed this experiment with two mountains of the same radius $R = \pi/9$. The mountains were both at latitude $\theta_c = \pi/6$,

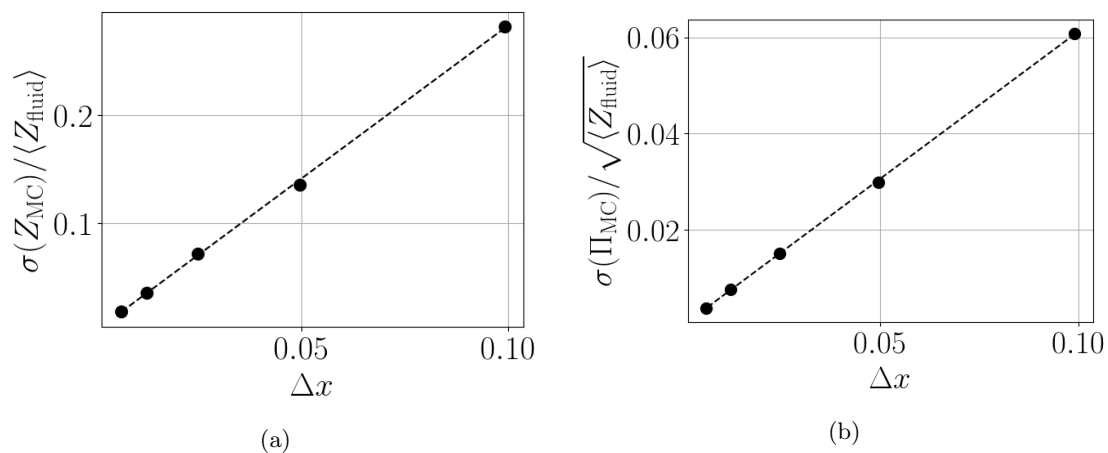


Figure 6: The standard deviations of the histograms such as those in Figure 5 of (a) $\Pi = \int_{\Omega} q \, d^2x$ and (b) $Z = \frac{1}{2} \int_{\Omega} q^2 \, d^2x$ as a function of resolution. This shows the convergence of the Gibbs distribution to the delta function as the grid spacing goes to zero.

but at longitudes $\lambda_{c1} = -\pi/4$ and $\lambda_{c2} = \pi/4$. Figures 7 and 8 show comparisons between the fluid and statistical simulations of mean ψ fields plotted after $T = 10^5$ time steps and $n = 10^5$ samples were taken. The third icosahedron refinement level was used, giving 642 q DOFs. For both the fluid and statistical simulations, the average fields are very similar.

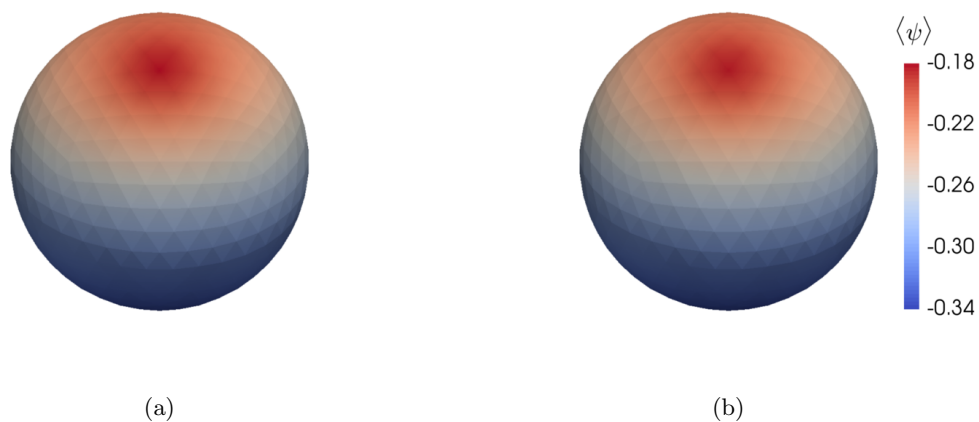


Figure 7: A comparison of the mean stream function ψ field generated over topography. In this case we used flow over a single mountain, and we show (a) the stochastic fluid simulation run for 10^6 steps and (b) 10^6 samples taken from the Metropolis algorithm. The plots are essentially the same, illustrating the prediction of the statistical theory.

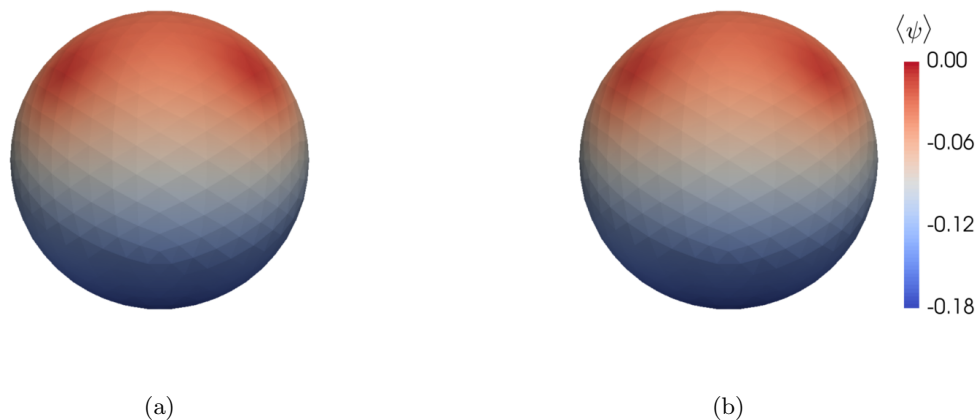


Figure 8: A comparison for the two-mountain case of the mean stream function ψ field generated by (a) the stochastic fluid simulation run for 10^6 steps and (b) 10^6 samples taken from the Metropolis algorithm. The plots are essentially the same, illustrating the prediction of the statistical theory.

6 Summary and Outlook

Holm's work of [1] gave the framework for a stochastic variational principle for QG, which was extended to derive the stochastic QG from the appropriate Lagrangian, before considering quantities conserved by this system. A finite element methods was presented to discretise the stochastic QG equation. Statistical predictions were then made about this numerical scheme following the approach of [12], which were tested by sampling using a Metropolis algorithm. The statistics generated by sampling the resulting Gibbs-like distribution compared with those averaged quantities from solving the stochastic equations of motion.

Acknowledgements. TMB was supported by the EPSRC Mathematics of Planet Earth Centre for Doctoral Training at Imperial College London and the University of Reading. CJC was supported by EPSRC grant EP/N023781/1.

References

- [1] D. D. Holm, “Variational principles for stochastic fluid dynamics,” in *Proc. R. Soc. A*, vol. 471, p. 20140963, The Royal Society, 2015.
- [2] D. D. Holm and V. Zeitlin, “Hamilton’s principle for quasigeostrophic motion,” *Physics of Fluids (1994-present)*, vol. 10, no. 4, pp. 800–806, 1998.
- [3] L. Onsager, “Statistical hydrodynamics,” *Il Nuovo Cimento (1943-1954)*, vol. 6, pp. 279–287, 1949.
- [4] R. H. Kraichnan, “Inertial ranges in two-dimensional turbulence,” *The Physics of Fluids*, vol. 10, no. 7, pp. 1417–1423, 1967.
- [5] R. H. Kraichnan, “Statistical dynamics of two-dimensional flow,” *Journal of Fluid Mechanics*, vol. 67, no. 01, pp. 155–175, 1975.
- [6] R. H. Kraichnan and D. Montgomery, “Two-dimensional turbulence,” *Reports on Progress in Physics*, vol. 43, no. 5, p. 547, 1980.
- [7] G. Carnevale, U. Frisch, and R. Salmon, “H theorems in statistical fluid dynamics,” *Journal of Physics A: Mathematical and General*, vol. 14, no. 7, p. 1701, 1981.
- [8] G. F. Carnevale, “Statistical features of the evolution of two-dimensional turbulence,” *Journal of Fluid Mechanics*, vol. 122, pp. 143–153, 1982.
- [9] R. Salmon, G. Holloway, and M. C. Hendershott, “The equilibrium statistical mechanics of simple quasi-geostrophic models,” *Journal of Fluid Mechanics*, vol. 75, no. 04, pp. 691–703, 1976.
- [10] G. F. Carnevale and J. S. Frederiksen, “Nonlinear stability and statistical mechanics of flow over topography,” *Journal of Fluid Mechanics*, vol. 175, pp. 157–181, 1987.
- [11] W. J. Merryfield, P. F. Cummins, and G. Holloway, “Equilibrium statistical mechanics of barotropic flow over finite topography,” *Journal of physical oceanography*, vol. 31, no. 7, pp. 1880–1890, 2001.
- [12] A. Majda and X. Wang, *Nonlinear dynamics and statistical theories for basic geophysical flows*. Cambridge University Press, 2006.
- [13] S. Dubinkina and J. Frank, “Statistical mechanics of Arakawa’s discretizations,” *Journal of Computational Physics*, vol. 227, no. 2, pp. 1286–1305, 2007.
- [14] S. Reich and C. Cotter, *Probabilistic forecasting and Bayesian data assimilation*. Cambridge University Press, 2015.
- [15] F. Rathgeber, D. Ham, L. Mitchell, M. Lange, F. Luporini, A. McRae, G.-T. Bercea, G. Markall, and P. Kelly, “Firedrake: automating the finite element method by composing abstractions,” 2016.
- [16] D. L. Williamson, J. B. Drake, J. J. Hack, R. Jakob, and P. N. Swarztrauber, “A standard test set for numerical approximations to the shallow water equations in spherical geometry,” *Journal of Computational Physics*, vol. 102, no. 1, pp. 211–224, 1992.